IEEE Access
Multidisciplinary ⋮ Rapid Review ⋮ Open Access Journal

Received 9 April 2023, accepted 21 April 2023, date of publication 28 April 2023, date of current version 18 September 2023.

Digital Object Identifier 10.1109/ACCESS.2023.3271518

RESEARCH ARTICLE

Fully Connected U-Net and Its Application on Reconstructing Successively Sampled Seismic Data

SHENGJUN LI[1], JIANHU GAO[1], JINYONG GUI[1], LUKUN WU[2], NAIHAO LIU[3], (Member, IEEE), DONGYANG HE[1], AND XIN GUO[1]

[1]PetroChina Research Institute of Petroleum Exploration and Development, Northwest, China National Petroleum Corporation (CNPC), Lanzhou, Gansu 730020, China
[2]School of Software Engineering, Xi'an Jiaotong University, Xi'an, Shaanxi 710049, China
[3]School of Information and Communications Engineering, Xi'an Jiaotong University, Xi'an, Shaanxi 710049, China

Corresponding authors: Jianhu Gao (gaojh@petrochina.com.cn) and Naihao Liu (naihao_liu@mail.xjtu.edu.cn)

This work was supported in part by the Prospective, Basic, and Strategic Technology Research Project of PetroChina under Grant 2021DJ0606; in part by the Science and Technology Project of PetroChina under Grant 2022KT1503; and in part by the National Natural Science Foundation of China under Grant 4197040204.

ABSTRACT One of the major hot topics in seismic data processing is the reconstruction of successively sampled seismic data. There are numerous traditional methods proposed for addressing this issue; however, they still have unavoidable drawbacks, such as high computational cost and sensitive tuning parameters. In this study, we suggest a deep learning model for reconstructing successively sampled seismic data, termed fully connected U-Net (FCU-Net). FCU-Net maintains the high-resolution representations by connecting the parallel different-resolution representations and repeating multi-scale fusion. Such a structure allows FCU-Net to successfully extract multi-scale information, which is beneficial for accurate seismic data reconstruction. Additionally, the extending subnetwork of FCU-Net contains a large number of feature channels and sufficient information interaction between different resolution representations via the composite cascades, which contributes to locating successively sampled traces with big gaps and then performing the seismic interpolation. To verify the effectiveness of FCU-Net, we compare it with state-of-the-art networks, i.e., U-Net and HRNet, using synthetic and field examples. The results show that FCU-Net performs best when interpolating successively sampled seismic data, proving its superiority and availability.

INDEX TERMS Successively sampled seismic data reconstruction, deep learning, U-Net, fully connected network.

I. INTRODUCTION

Due to the constraints on the acquisition condition, the cost limitations, and the dead traces, the received seismic data is often sampled [1], [2]. Sampled seismic data reconstruction is one of the key and tough tasks in seismic data processing [3], [4], which benefits further seismic data processing and interpretation, e.g., coherent and incoherent noise attenuation [5], [6], [7], [8], [9], geological structure characterization [10], [11], [12], attribute analysis [13], [14], [15], [16], fault and horizon interpretation [17], [18], [19], lithology recognition [20], [21], [22], etc. The sampled seismic data can be mainly divided into randomly and successively sampled cases [23]. Note that interpolating the successively sampled seismic data is a more difficult task than interpolating the randomly sampled case. Therefore, in this study, we pay attention to the successively sampled seismic data reconstruction.

With the development of signal processing and computational science, there are kinds of methods proposed for interpolating the successively sampled seismic data. The traditional methods can be divided into four categories, mainly including wave equation-based method [24], [25], prediction error filter-based method [23], [26], transform-based

The associate editor coordinating the review of this manuscript and approving it for publication was Vivek Kumar Sehgal.

method [27], [28], and rank reduction based method [29], [30]. These above reconstruction approaches are proposed for different application scenarios. Nevertheless, there are several unavoidable limitations in these traditional reconstruction methods. First, we often face hundreds of pre-stack seismic gathers when addressing seismic reconstruction; therefore, the high computational cost of traditional methods should be effectively relaxed and addressed. Second, there are usually several key parameters that need to be manually defined after several tests. Third, these traditional methods often require prior assumptions, which are difficult to obtain, especially when processing field data.

Recently, machine learning and deep learning are successfully adopted for addressing geological issues [31], [32], [33], [34], [35], [36], which are also utilized for seismic data reconstruction [37], [38], [39], [40], [41], [42]. Among these deep learning based models, U-Net is a commonly used one that was originally proposed for medical image segmentation [43]. Especially, numerous feature channels are introduced in the upsampling stage of U-Net to propagate contextual information, which enables it to precisely localize objects. Additionally, the concatenation operation can also help U-Net to fuse multi-scale information. In light of these strengths, U-Net is utilized for promoting seismic processing and interpretation [44], [45], [46], [47], which is also used for interpolating sampled seismic data [48]. For example, He et al. proposed a multi-stage training process to build multiple U-net models for successively sampled trace interpolation [49]. To restore irregularly and regularly sampled 3-D data on several typical seismic data sets, especially those with high sampled percentages or large gaps, Fang et al. established an artificial neural network (ANN) based on an end-to-end U-Net encoder-decoder style 3-D convolutional neural network (CNN) [50]. In addition, many networks with U-Net as the backbone have been proposed. Based on U-Net, Wang et al. proposed an eight-layer residual learning network (ResNets) with improved deep backpropagation properties to aid in the highly accurate reconstruction of irregularly sampled traces [3]. Liu et al. proposed a wavelet-based network for reconstructing seismic data by using U-Net as its backbone [2]. Unfortunately, the shallow high-resolution features in the encoder are only propagated to the corresponding layers in the decoder via the concatenation operation in U-Net. And, each pooling operation will halve the size in the encoder, indicating that the received shallow feature information is constrained. Due to the insufficient multi-scale information obtained by U-Net, the detailed features may be lost or the images may be distorted. There are several state-of-the-art models proposed for addressing this [51], [52]. For example, Wang et al. proposed a High-Resolution Network (HRNet) [53], which has been initially employed to address computer vision issues. HRNet encourages high- and low- resolution representations to advance in the network in parallel and repeating multiple-resolution representation fusion between levels, allowing it to fully utilize multi-scale information to boost the model's accuracy. However, HRNet uses a deep supervision technique rather than an extending subnetwork for precise localization like U-Net in the decoder. For seismic data reconstruction tasks, it is vital to locate the sampling locations, while HRNet struggles with this.

In this study, we propose a fully connected U-Net (FCU-Net) for addressing successively sampled seismic data. The main contributions of this study are summarized as follows.

1) FCU-Net is a parallel variant of U-Net, which completes the multi-resolution information transmission through composite cascading between several levels, benefiting the efficient extraction of multi-scale information.
2) Many multi-scale feature channels are introduced by the FCU-Net expanding subnetwork, which is beneficial for the localization of successively sampled traces and stable model training.
3) We utilize synthetic and field data to test the effectiveness of FCU-Net. Moreover, we provide detailed qualitative and quantitative comparisons with state-of-the-art deep learning models.

In the following sections, we first introduce the related U-Net and HRNet. Following that, we present the detailed architecture of our proposed FCU-Net. Afterward, we implement the experiments on synthetic and field data sets, both of which suffer from the successively sampled issue. After comparing the proposed model with U-Net and HRNet in reconstructing successively sampled seismic data, we present their qualitative and quantitative results and detailed analyses. Finally, we provide several discussions and the main conclusions of this study.

II. METHODOLOGY

A. U-NET

The architecture of U-Net can be divided into two parts, i.e., the contracting subnetwork (encoder) for obtaining contextual information and the expanding subnetwork (decoder) for precise localization [43], which is more or less symmetric to the contracting subnetwork. As a consequence, the U-shaped architecture is called U-Net. Note that U-Net is a fully convolutional network (FCN). Nevertheless, compared with the general FCN, U-Net has two main advantages. One is the symmetric expanding subnetwork, which yields a large number of feature channels, allowing the network to propagate context information to higher-resolution layers. The second is that U-Net connects the encoder and the decoder via the concatenation operation, preventing vanishing gradients and fusing the feature representations of various levels. Aided by the superior performance, U-Net is applied in incomplete seismic data reconstruction, which can be expressed as

$$\mathbf{x} = h(f(\mathbf{x}_{raw}; \theta)), \tag{1}$$

where $\mathbf{x}_{raw}$ denotes the raw incomplete seismic data as the input; θ represents the convolution kernel weights, bias, and hyperparameters in the network; $h(\cdot)$ is the activation

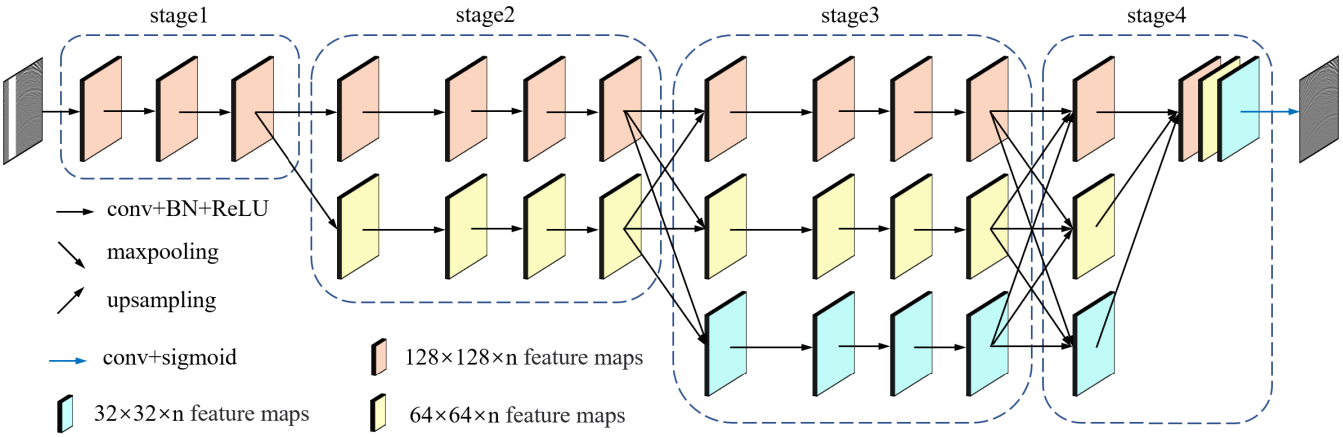

FIGURE 1. The simplified architecture of HRNet [53], which is divided into 4 stages to make the process of feature fusion between various levels explicitly obvious. In particular, the feature maps at different levels are colored to differentiate. The light orange, light yellow, and light blue color blocks represent $128 \times 128 \times n$, $64 \times 64 \times n$, and $32 \times 32 \times n$ feature maps, respectively, where n is the number of channels.

function. $\mathbf{x}$ presents the predicted output. Here, $f(\mathbf{x}_{raw}; \theta)$ indicates a neural network suggested for solving seismic data reconstruction.

In U-Net, the deeper, high-semantic features are the focus of the lower convolutional layers, while the shallow, high-resolution features are the focus of the higher convolutional layers. In the effort of reconstructing seismic data, both shallow and deep characteristics must be acquired. Deep features can be effectively propagated by U-Net, but shallow features can only be spread through concatenation. Also, each downsampling reduces the scale by half, demonstrating the inadequacy of the information communicated through concatenation. In short, the skip connection structure of U-Net, which is close to series, does not make effective use of shallow features, which will lead to the loss of detailed features or distortions of the input image.

B. HRNet

High-Resolution Network (HRNet) is first proposed to address computer vision problems [53]. The parallel structure of HRNet can effectively solve the problem of the under-utilization of shallow features of U-Net. Definitely, HRNet first encodes the input image into a low-resolution representation via subnets formed by serial high- and low-resolution convolutions, such as Residual Network (ResNet) and Visual Geometry Group Network (VGGNet), and then recovers the high-resolution representation via the encoded low-resolution representation [33]. While HRNet can maintain high resolution representations throughout the whole process, it is called High-Resolution Network. HRNet maintains high-resolution representations by connecting parallel different-resolution representations and repeating multi-scale fusion. As a consequence, the extracted high-resolution representations are not only informative but also spatially accurate. Figure 1 shows a simplified architecture of HRNet [53]. It should be noted that HRNet in this study actually refers to HRNetV2, which fuses multi-scale features of different resolution representations in the final output to facilitate image fidelity.

For simplicity, we divide HRNet into four stages in Figure 1. Here, the light orange, light yellow, and light blue color blocks represent $128 \times 128 \times n$, $64 \times 64 \times n$, and $32 \times 32 \times n$ feature maps, respectively, where n is the number of channels. In each stage, different resolution representations are propagated in parallel. On the other hand, the multi-scale repetitive fusion is carried out among different stages, which improves the ability of image detail extraction and processing. Note that as the network levels increase, this fusion behavior gets more sophisticated, facilitating communication between low-level semantic features and high-level abstract features to promote the fitting of the network model. In addition, in stage 4, the output of the parallel low-resolution subnet is first up-sampled to the size of the high-resolution subnet, and then four branches of the same size are connected through a cascade operation, and finally, a 1×1 convolution (the remaining convolution kernels are 3×3 in Figure 1) is performed to get the final result. It is worth noting that stage 4 is actually a deep supervision strategy, which improves the transparency and directness of each hidden layer. Note that the deep supervision is originally proposed to solve the classification task, without considering the characteristics of seismic data, and the multi-scale features are not further integrated and learned by the decoder, which leads to the location of big gaps of incomplete seismic data being difficult to determine.

C. FULLY CONNECTED U-NET

We suggest a fully connected U-Net based on U-Net and HRNet from the preceding subsections, called fully connected U-Net (FCU-Net). FCU-Net takes advantage of U-Net and HRNet and can extract multi-resolution features more effectively, which will be beneficial in reconstructing

successively sampled seismic data. Figure 2 shows the simplified structure of the proposed FCU-Net and Table 1 presents its detailed operations and hyperparameters. Note that the light orange, light yellow, and light blue color blocks represent $128 \times 128 \times n$, $64 \times 64 \times n$, and $32 \times 32 \times n$ feature maps, respectively, where n is the number of channels. Afterward, seismic data reconstruction via the suggested FCU-Net can be denoted as

$$\mathbf{x} = h_{\text{sigmoid}}\left(f_{FC}\left(\mathbf{x}_{\text{raw}}\,;\theta\right)\right), \tag{2}$$

where $\mathbf{x}_{raw}$ and $\mathbf{x}$ denote the input sampled seismic data and the predicted output. $f_{FC}(\cdot)$ denotes the suggested FCU-Net. θ presents the convolution kernel weights, bias, and hyperparameters in FCU-Net. The activation function is selected as the sigmoid function, denoted as $h_{\text{sigmoid}}(\cdot)$.

While reconstructing sequentially sampled seismic data, FCU-Net has the following advantages by taking into account the structures of U-Net and HRNet.

1) In FCU-Net, different resolution representatives within each stage are processed in parallel. At the same time, repeated multi-scale fusions are achieved between different stages based on composite cascades. Visually, FCU-Net actually fills the ''hollow'' of U-Net. Such a structure makes full use of shallow high-resolution representatives. It facilitates multi-scale information interaction, which can preserve more detailed features of the sampled image and obtain more accurate interpolated results. Furthermore, it provides more alternative paths for gradient feedback during network training, which allows the model to fit in a more reasonable direction and then helps to recover incomplete seismic data.

2) Structurally, the proposed FCU-Net changes stage 4 of HRNet, as shown in the red dashed box in Figure 2. Note that when reconstructing the successively sampled seismic data, the location of big gaps is significant for the reconstruction results. Stage 4 of FCU-Net constitutes a decoder, which introduces a large number of feature channels into the model and further enhances the integration and interaction of multi-scale feature information during the decoding process. Such an improvement helps the model learn more critical features, especially locating big gaps of incomplete seismic data, which would result in finer and more satisfactory reconstruction results.

D. EVALUATION METRICS

We introduce evaluation metrics to quantitatively test the effectiveness of the proposed model, including Mean Absolute Error (MAE) [54], Structure Similarity Index Measure (SSIM) [55], and signal-to-noise ratio (SNR) [56]. Suppose that $\mathbf{x_i}$ and $\mathbf{y_i}$ represent the i-th predicted output and the i-th raw complete data, $\mathbf{x}$ is the predicted result and $\mathbf{y}$ is the raw complete data. Note that, after obtaining $\mathbf{x}$, we adopt all traces of $\mathbf{x}$ to calculate evaluation metrics. Afterward, these evaluation indicators are explained as follows.

Mean Absolute Error (MAE) [54]:

$$MAE = \frac{1}{n}\sum_{i=1}^{n}\left|\mathbf{x_i} - \mathbf{y_i}\right|, \tag{3}$$

where n represents the number of the samples, $[0, +\infty)$. When the predicted value is completely consistent with the ground truth, MAE is equal to 0, which indicates obtaining a perfect model. And, the larger the error, the larger the value [54].

Structure Similarity Index Measure (SSIM) [55]: SSIM is a measurement for describing the similarity between two images [55]. SSIM of two images $\mathbf{x}$ and $\mathbf{y}$ can be calculated as

$$SSIM(\mathbf{x}, \mathbf{y}) = \frac{\left(2\mu_{\mathbf{x}}\mu_{\mathbf{y}} + c_1\right)\left(2\sigma_{\mathbf{xy}} + c_2\right)}{\left(\mu_{\mathbf{x}}^2 + \mu_{\mathbf{y}}^2 + c_1\right)\left(\sigma_{\mathbf{x}}^2 + \sigma_{\mathbf{y}}^2 + c_2\right)}, \tag{4}$$

where $\mu_{\mathbf{x}}$ and $\mu_{\mathbf{y}}$ present the averages of $\mathbf{x}$ and $\mathbf{y}$, $\sigma_{\mathbf{x}}^2$ and $\sigma_{\mathbf{y}}^2$ indicate the variances of $\mathbf{x}$ and $\mathbf{y}$. $\sigma_{\mathbf{x},\mathbf{y}}$ is the covariance of $\mathbf{x}$ and $\mathbf{y}$. $c_1 = (k_1 L)^2$ and $c_2 = (k_2 L)^2$ are both constant values used to maintain the stability, where $k_1 = 0.01$ and $k_2 = 0.03$. L is the dynamic range of the pixel values. SSIM of two images is between 0 and 1, when SSIM is closer to 1, the reconstructed image is more fidelity.

Signal to Noise Ratio (SNR) [56]:

$$\text{S/N(dB)} = 20\log_{10}\frac{\|\mathbf{y}\|_2}{\|\mathbf{y} - \mathbf{x}\|_2}, \tag{5}$$

The larger the SNR denotes the better the restored image quality [56].

E. TRAINING DETAILS

During model training, Tensorflow-GPU deep learning library 2.4.0 and Keras 2.4.3 on Python 3.6 are used to build all models. The experiments are implemented using NVIDIA GTX 3090. In addition, we use an Adam optimizer with default settings. Furthermore, the layers adopt the commonly used Rectified Linear Unit (ReLU) [57] activation function except for the last layer of the network, which is activated by the sigmoid function. Meanwhile, we use the MSE loss [58] in Equation (6) to monitor the error between the raw complete data $\mathbf{y}$ and the predicted result $\mathbf{x}$.

$$MSE = \frac{1}{n}\sum_{i=1}^{n}\left(\mathbf{x_i} - \mathbf{y_i}\right)^2, \tag{6}$$

where $\mathbf{x_i}$ and $\mathbf{y_i}$ represent the i-th predicted result and the i-th label. n represents the number of the samples, $[0, +\infty)$. When MSE is employed as the loss function, the model is gradually fitting as its value gradually declines.

III. SYNTHETIC EXAMPLES

The synthetic data used in this study is the public SEG C3 data set,[1] whose temporal sampling interval and temporal sampling number are 8 ms and 625. We randomly select

[1] https://wiki.seg.org/wiki/SEG_C3_NA

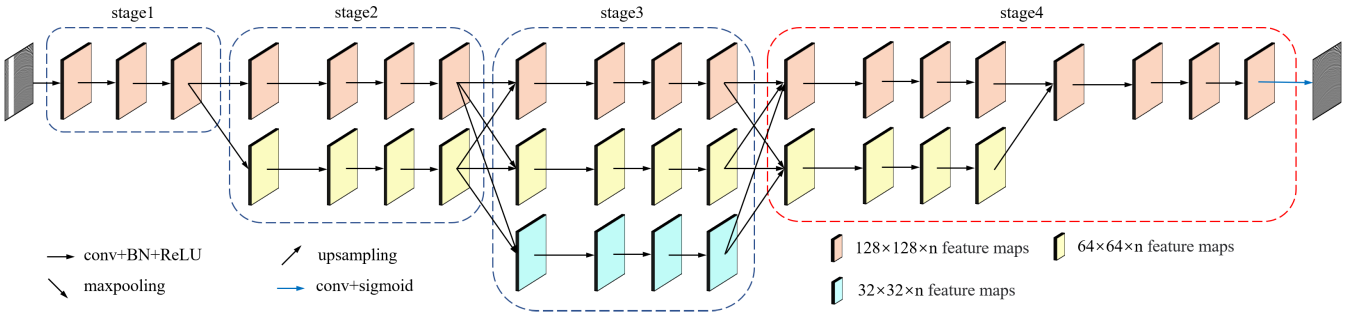

FIGURE 2. The simplified architecture of the proposed FCU-Net. The color and stages of the feature maps are similar to those in Figure 1. The light orange, light yellow, and light blue color blocks represent 128 × 128 × *n*, 64 × 64 × *n*, and 32 × 32 × *n* feature maps, respectively, where *n* is the number of channels.

TABLE 1. The specific operations and hyperparameters of the proposed FCU-Net. It should be noted that the layer names in the table follow that the first number represents the network level and the second number represents the order of the feature layer. For example, level1_3 represents the third feature layer in the first level. In addition, conv block represents the combination of convolution, BN, and ReLU operations.

Layer name	Operation	Input size	Output size
input	——	——	(128, 128, 1)
level1_3	conv block (input)× 3	(128, 128, 1)	(128, 128, 32)
level1_7	conv block (level1_3)× 4	(128, 128, 32)	(128, 128, 32)
level2_1	maxpooling(level1_3)	(128, 128, 32)	(64, 64, 32)
level2_4	conv block (level2_1)× 3	(64, 64, 32)	(64, 64, 64)
level1_8	concatenate (conv block (level1_7), upsampling (level2_4))	(128, 128, 32), (64, 64, 64)	(128, 128, 96)
level2_5	concatenate (maxpooling (level1_7), conv block (level2_4))	(128, 128, 32), (64, 64, 64)	(64, 64, 96)
level3_1	concatenate (maxpooling (level1_7)× 2, maxpooling (level2_4))	(128, 128, 32), (64, 64, 64)	(32, 32, 96)
level1_11	conv block (level1_8)× 3	(128, 128, 96)	(128, 128, 32)
level2_8	conv block (level2_5)× 3	(64, 64, 96)	(64, 64, 64)
level3_4	conv block (level3_1)× 3	(32, 32, 96)	(32, 32, 128)
level1_12	concatenate (conv block (level1_11), upsampling (level2_8)), upsampling (level3_4)× 2)	(128, 128, 32), (64, 64, 64), (32, 32, 128)	(128, 128, 224)
level2_9	concatenate (maxpooling (level1_11), conv block (level2_8)), upsampling (level3_4))	(128, 128, 32), (64, 64, 64), (32, 32, 128)	(64, 64, 224)
level1_15	conv block (level1_12)× 3	(128, 128, 224)	(128, 128, 32)
level2_12	conv block (level2_9)× 3	(64, 64, 224)	(64, 64, 64)
level1_16	concatenate (conv block (level1_15), upsampling (level2_12))	(128, 128, 32), (64, 64, 64)	(128, 128, 96)
level1_19	conv block (level1_16)× 3	(128, 128, 96)	(128, 128, 32)
output	conv+sigmoid(level1_19)	(128, 128, 32)	(128, 128, 1)

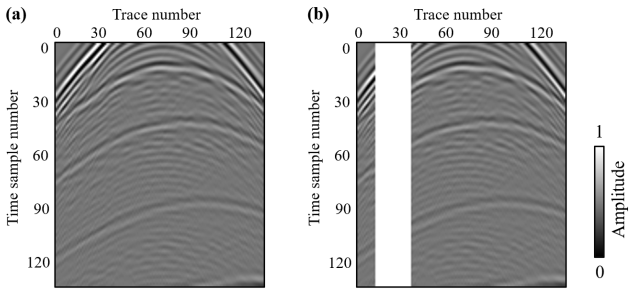

FIGURE 3. A synthetic data example from the blind test data set, (a) ground truth and (b) the input data after removing seismic traces with a big gap.

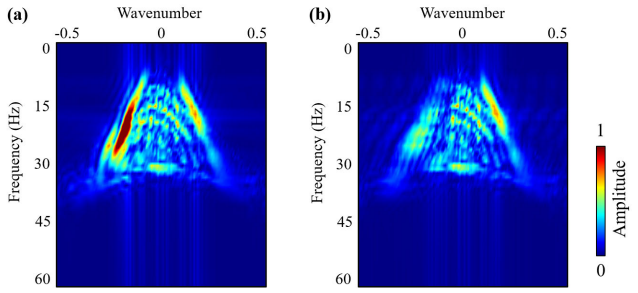

FIGURE 4. The $f - k$ spectra of the images in Figure 3, (a) ground truth, and (b) input data after removing seismic traces with a big gap.

TABLE 2. The parameters, FLOPs, and training time of different models.

Model	parameters (M)	FLOPs (G)	training time (h)
U-Net	**3.12**	**6.32**	1.27
HRNet	5.92	10.50	2.25
FCU-Net	4.71	11.89	2.43

8000 patches of 128 × 128 from the SEG C3 data set and all extracted patches are then normalized as [0, 1] by using the Min-Max normalization. Next, we divide these 8000 patches into 50% training set with 4000 patches, 25% validation set with 2000 patches, and 25% blind test set with 2000 patches, as our synthetic data set. Since FCU-Net is a supervised deep learning model, each patch contains the raw complete data $\mathbf{y}$ as the ground truth of the network, and after removing seismic traces with a big gap, the sampled data as the input data $\mathbf{x}_{\text{ori}}$, as shown in Figure 3(a) and 3(b). In addition, Figure 4 shows the corresponding $f - k$ spectra of the images in Figure 3. Note that x-axis and y-axis represent the normalized wavenumber and frequency. As observed in Figure 4, there is a significant loss in the amplitude of data after removing seismic traces with a big gap, therefore, we must restore seismic valid amplitudes to facilitate subsequent seismic data interpretation. In addition, the proportion of the sampled big gap is randomly set to 10%-30%, whose location is also random.

Following the ablation tests in Figure 5 and Figure 6, it can be easily found that, when the initial learning rate and

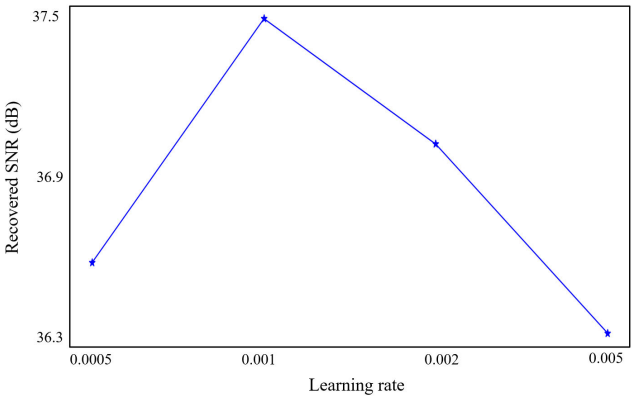

FIGURE 5. Recovered SNR of different learning rates based on synthetic data set with successively sampled traces.

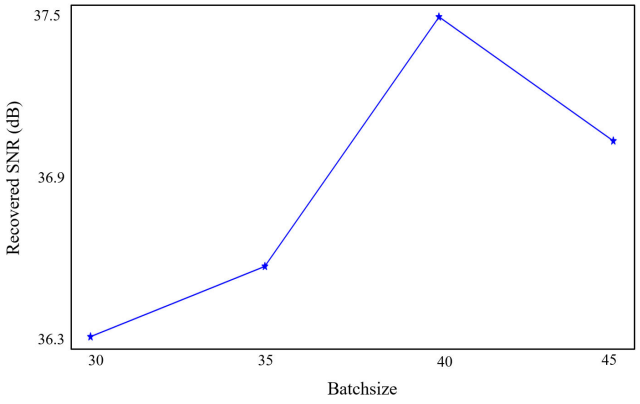

FIGURE 6. Recovered SNR of different batch sizes based on synthetic data set with successively sampled traces.

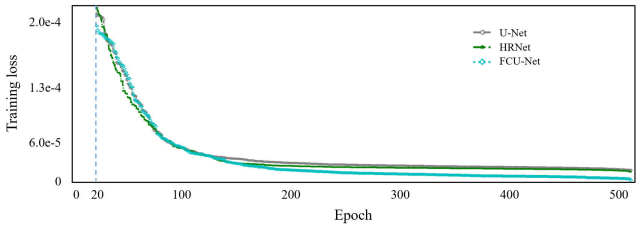

FIGURE 7. The training MSE loss curves of different deep learning models on the training data set of the successively sampled synthetic data with a big gap.

batch size are adjusted to 0.001 and 40, the recovered SNR value of the training model for the sampled data can achieve a higher value. After applying these settings and training deep learning models for 500 epochs, the loss curves of all deep learning models do not drop further and achieve convergence, as shown in Figure 7. It should be noted that to better compare the performance of the proposed FCU-Net, we also train U-Net and HRNet, which adopt the same 3-level structure as FCU-Net. Here, the gray circle, the green star, and the cyan diamond represent the MSE loss curves of U-Net, HRNet, and FCU-Net. Specially, we show the loss curves of these deep learning models from 20-th epoch

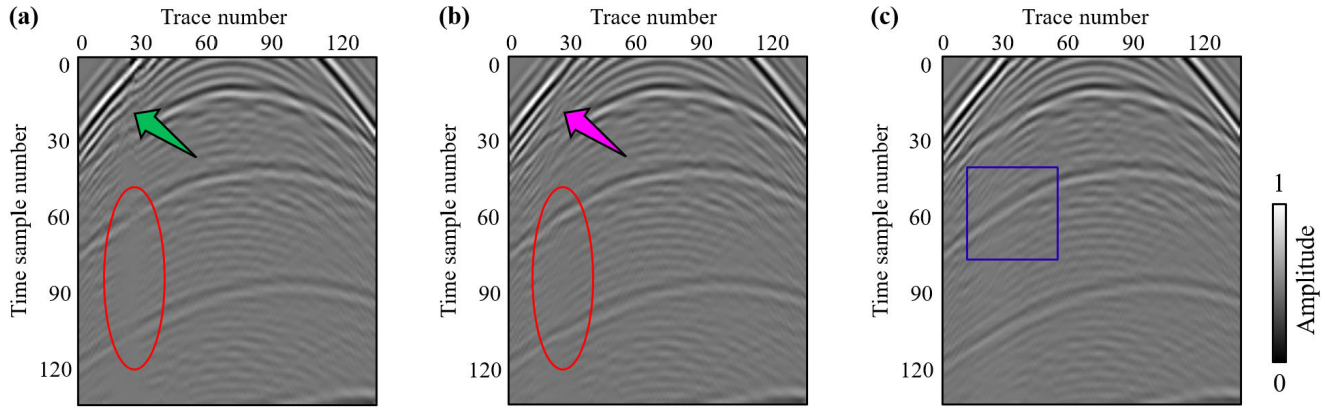

FIGURE 8. The reconstructed results of the successively sampled example in Figure 3(b) using (a) U-Net, (b) HRNet, and (c) FCU-Net.

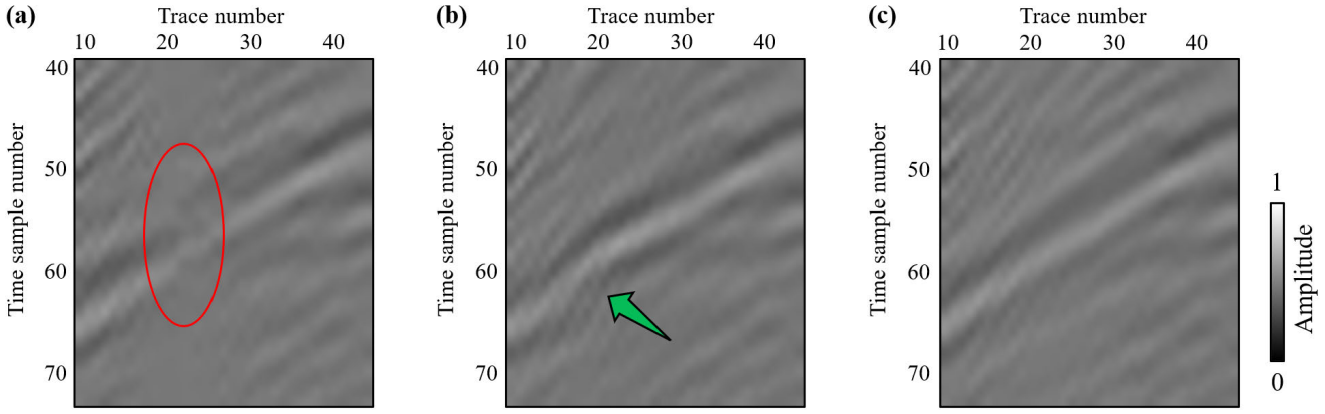

FIGURE 9. The enlarged images indicated by the blue rectangle in Figure 8(c), calculated using (a) U-Net, (b) HRNet, and (c) FCU-Net.

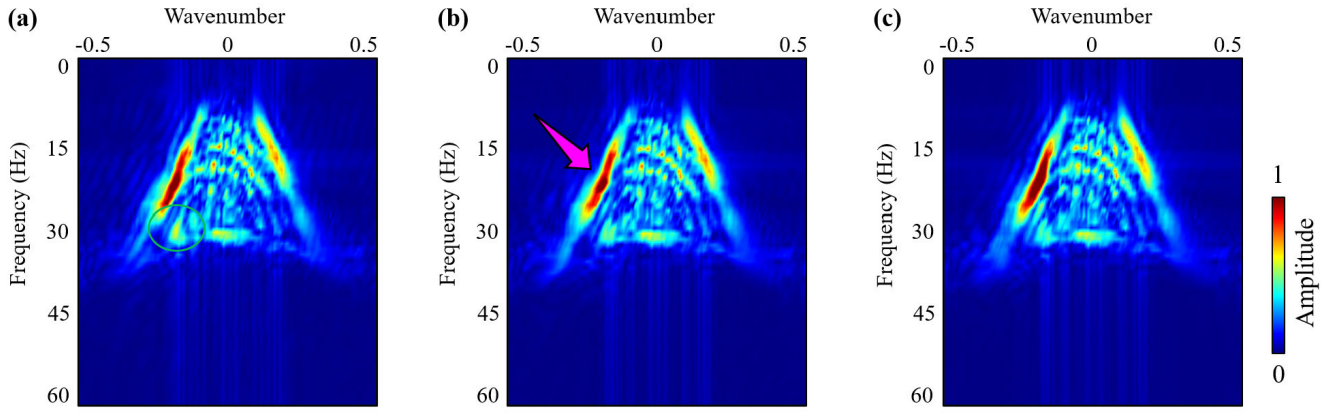

FIGURE 10. The $f - k$ spectra of the images in Figure 8, (a) U-Net, (b) HRNet, and (c) FCU-Net.

so that the final convergence effect can be clearly seen. Based on these loss curves, we can find that we obtain three well-trained deep learning models. Furthermore, we provide the parameters, floating-point operations (FLOPs), and training time of different deep learning models in Table 2. Note that the larger number of parameters indicates more space complexity, while the larger FLOPs indicate more time complexity. These values in Table 2 indicate that U-Net shows less model complexity and less time complexity, compared with HRNet and our model. Our model shows similar complexity to HRNet, which is the main limitation of our model.

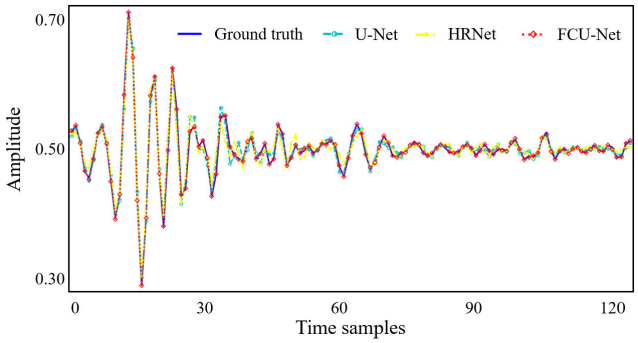

FIGURE 11. A synthetic trace example of consecutively missing synthetic data from Figure 8, with the trace number 13. The blue solid, cyan circle, yellow star, and red diamond curves present the ground truth and the restored traces computed using U-Net, HRNet, and FCU-Net, respectively.

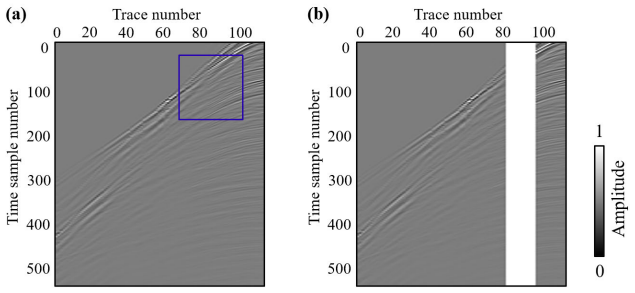

FIGURE 12. A field data example from the blind test data set, (a) ground truth, and (b) the input data after removing seismic traces with a big gap.

TABLE 3. Quantitative comparisons of different models on successively sampled synthetic data.

Model	MAE	SSIM	SNR
U-Net	3.1353e-03	0.9725	37.0048
HRNet	2.9803e-03	0.9732	37.1067
FCU-Net	**2.9171e-03**	**0.9750**	**37.4145**

Figure 8 depicts the reconstructed results of the successively sampled image in Figure 3(b), predicted using (a) U-Net, (b) HRNet, and (c) FCU-Net. From the reconstruction results in Figure 8, we can see that U-Net can reconstruct sampled traces adjacent to the known traces. However, the middle part of successively sampled traces with a big gap is not reconstructed, indicated by the red circle in Figure 8(a). In addition, the strong valid amplitudes restored using U-Net are inconsistent with the corresponding part of ground truth in Figure 3(a), denoted by the green arrow in Figure 8(a). Moreover, it can be observed that successively sampled traces reconstructed using HRNet still show significant errors, especially as shown by the red circle in Figure 8(b). Meanwhile, the interpolated result in Figure 8(b) has obvious amplitude loss at the original strong amplitude part, as highlighted by the pink arrow. Comparatively, it can be easily found from Figure 8(c) that the reconstructed data using FCU-Net is more accurate than the interpolated images using U-Net and HRNet, especially at the successively sampled parts. These above discussions demonstrate that FCU-Net can promote model training and train a better model for reconstructing the successively sampled seismic data. Furthermore, Figure 9 shows the corresponding enlarged images presented by the blue rectangle in Figure 8(c). Among them, the interpolated result calculated using U-Net loses most of the valid signals, indicating that it produces a large error, as presented by the red circle in Figure 9(a). However, as denoted by the green arrow in Figure 9(b), HRNet visibly restores more seismic traces, however, the result is inconsistent and inaccurate. Whereas, FCU-Net is able to reconstruct the most stable and comprehensive seismic traces in Figure 9(c).

Additionally, the $f-k$ spectra of the images in Figure 8 are calculated and shown in Figure 10(a), 10(b), and 10(c), where the vertical axis denotes the frequency and the horizontal axis represents the wavenumber. Figure 10(a) demonstrates that, while the image interpolated using U-Net can restore some of the valid amplitudes, there is still a clear difference compared with ground truth, particularly indicated by the green circle. In addition, the $f-k$ spectrum of the interpolated data using HRNet recovers more accurate valid amplitudes than that of U-Net, however, still suffers from the valid amplitude loss, as indicated by the pink arrow in Figure 10(b). Finally, Figure 10(c) shows that FCU-Net can successfully restore the missing amplitude information and achieve superior reconstructed results. Afterward, we display the synthetic trace example of the consecutively missing synthetic data in Figure 11, extracted from Figure 8 with the trace number 13. The blue solid, cyan circle, yellow star, and red diamond curves present the ground truth and the restored traces computed using U-Net, HRNet, and FCU-Net. Compared with U-Net and HRNet, FCU-Net's restored trace is closer to the ground truth and its error is less, which further proves its availability. Furthermore, U-Net, HRNet, and FCU-NET are quantitatively compared in Table 3 using MAE, SSIM, and SNR between the interpolated results and the ground truth. Table 3 makes it clear that, in comparison with U-Net and HRNet, FCU-Net achieves lower MAE and higher SSIM and SNR, indicating that FCU-Net performs best.

IV. FIELD DATA APPLICATIONS

After testing our proposed method on synthetic data, we then adopt the field data set to confirm the proposed model's effect and implement detailed comparisons with U-Net and HRNet. For the field data set, we randomly select 4000 patches from the Mobil Avo Viking Graben Line 12 field data set,[2] each of which has a size of 512 × 112. Note that the time sampling interval and the spatial sampling interval are 4 ms and 25 m. Next, we divide these 4000 patches into 2000, 1000, and 1000, respectively, for 50% training set, 25% validation set, and 25% blind test set. Additionally, these data sets are normalized as [0, 1] by using the Min-Max normalization.

[2]https://wiki.seg.org/wiki/Mobil_AVO_viking_graben_line_12

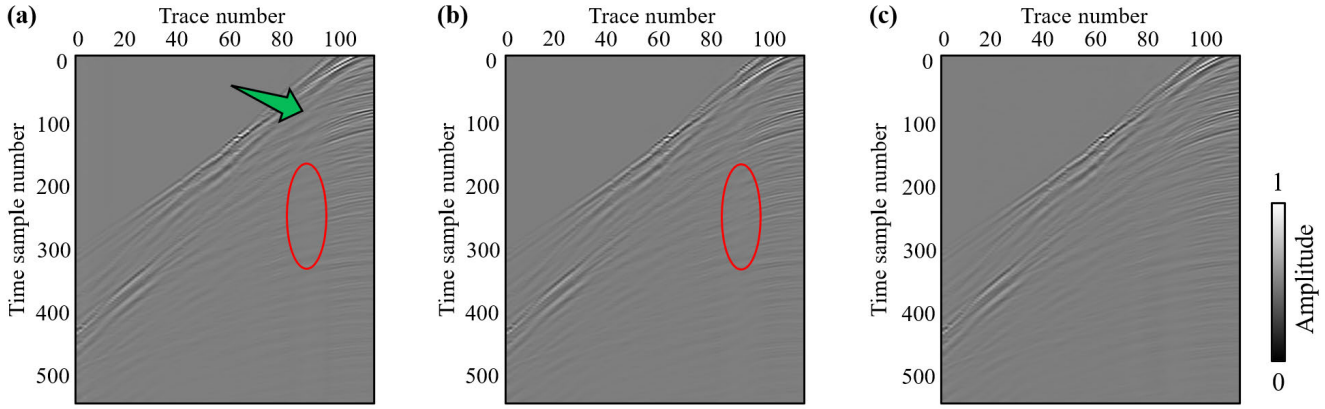

FIGURE 13. The reconstructed results of the successively sampled example in Figure 12(b) using (a) U-Net, (b) HRNet, and (c) FCU-Net.

TABLE 4. Quantitative comparisons of different models on successively sampled field data.

Model	MAE	SSIM	SNR
U-Net	2.2746e-03	0.9908	41.9436
HRNet	1.6984e-03	0.9911	43.0149
FCU-Net	**1.3678e-03**	**0.9921**	**44.0601**

Furthermore, by randomly sampling 10%-30% of the successively seismic traces from the raw complete data $\mathbf{y}$ as ground truth, we obtain the corresponding incomplete data $\mathbf{x}_{ori}$ as the input data of networks, as shown in Figure 12. Note that all the training details in this field case are identical to those in the synthetic case.

By applying the trained deep learning models to the input data after removing seismic traces with a big gap in Figure 12(b), we obtain the reconstruction results using U-Net, HRNet, and FCU-Net, as shown in Figure 13(a), 13(b), and 13(c). We can get several significant conclusions by analyzing the reconstruction results in Figure 13. First, U-Net recovers some valid sampled traces but fails to retain more amplitude details, which makes its interpolated result very fuzzy, especially at the area represented by the red circle in Figure 13(a). Consequently, the relative amplitude relationship of the ground truth in Figure 12(a) is not preserved in the interpolated component of U-Net, as highlighted by the green arrow in Figure 13(a). Second, when compared with ground truth in Figure 12(a), the data interpolated using HRNet still yields apparent errors, such as the area enclosed by the red circle in Figure 13(b). Finally, we find that the FCU-Net based reconstructed data is more continuous and recovers more detailed amplitudes than U-Net and HRNet based interpolated data.

Afterward, we further assess the reconstruction performance by analyzing the blue rectangle area marked in Figure 12(a). Figure 14 and Figure 15 represent the enlarged version of Figure 12 and Figure 13, extracted from the blue rectangle area indicated in Figure 12(a). We may safely draw

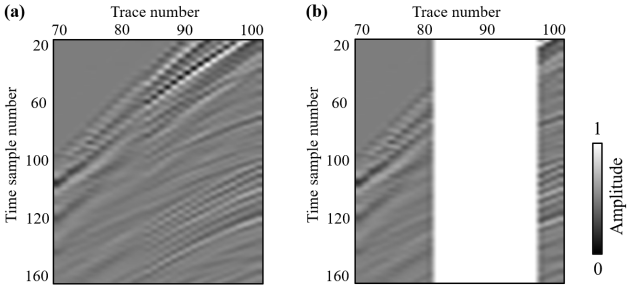

FIGURE 14. The enlarged images denoted by the blue rectangle in Figure 12, (a) ground truth, and (b) the input data after removing seismic traces with a big gap.

the same conclusion as before from comparing Figure 15, i.e., the image interpolated using FCU-Net is more accurate and contains more detailed amplitudes than those interpolated using U-Net and HRNet. For example, U-Net misses a lot of the details of the raw complete data in Figure 14(a), as circled by the red circle in Figure 15(a). Moreover, the relative amplitude relationship between successive traces at the reconstructed area is irrational, especially as indicated by the green arrow in Figure 15(a). Although HRNet outperforms U-Net in terms of its multi-scale fusion capability, it still has a significant error when compared with ground truth in Figure 14(a), and its image is plainly deformed, as represented by the red circle in Figure 15(b). Fortunately, our FCU-Net can fuse multi-scale information and accurately locate successively sampled traces, which makes it possible to train a model with good interpolation performance. As a result, FCU-Net produces the most refined and fidelity reconstruction results, as seen in Figure 15(c). Furthermore, we present a quantitative comparison of different deep learning models in Table 4. As shown in the bold text, the metrics calculated between FCU-Net based reconstructed results and ground truth all achieve the best results, i.e., lower MAE and higher SSIM and SNR. All of these aforementioned test results and analyses completely demonstrate the effectiveness, availability, and validity of FCU-Net in reconstructing successively

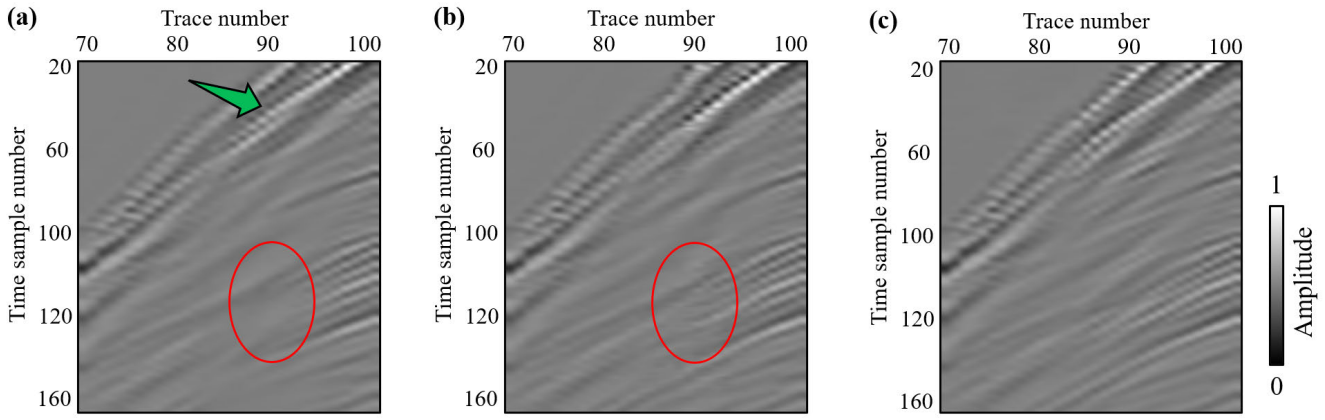

FIGURE 15. The enlarged reconstruction images indicated by the blue rectangle in Figure 12(a), i.e., the reconstructed results of Figure 14(b) predicted using (a) U-Net, (b) HRNet, and (c) FCU-Net.

sampled seismic data benefiting from its multi-scale information fusion capability and successively sampled traces location capability.

V. CONCLUSION

We suggest a fully connected U-Net (FCU-Net) to handle the problem of reconstructing the successively sampled traces with a big gap. Specifically, we connect different resolution representations in parallel and perform repeating multi-scale fusion in FCU-Net, which maintains high-resolution representations throughout the process. Seismic data reconstruction benefits from the effective use of the shallow high-resolution features and deep high-semantic features of the input image. Furthermore, FCU-Net features a symmetric structure that is comparable to U-Net, i.e., the contracting subnetwork for obtaining contextual information and the expanding subnetwork for precise localization, which is better for extracting multi-scale features and locating successively sampled traces. The numerical examples of synthetic and field data demonstrate that, in both qualitative and quantitative outcomes, FCU-Net beats the state-of-the-art networks, i.e., U-Net and HRNet. This validates the superiority and utility of FCU-Net in reconstructing successively sampled seismic data.

However, the limitations of the proposed model are still worth addressing in the future. First, the supervised deep learning model FCU-Net is suggested for tackling seismic data reconstruction. In some instances, particularly those involving field data, collecting ground truth labels for model training might be costly or challenging. Therefore, developing a high-performance unsupervised or semi-supervised deep learning model for interpolating sampled seismic data will thus be one of the next issues. In addition, FCU-Net has plenty of potential and can be used for various geological applications. For instance, it can be utilized to handle irregularly sampled seismic data reconstruction or attenuate random noise given its powerful multi-scale extraction capabilities and precise localization capability.

ACKNOWLEDGMENT

The authors would like to thank the Sandia National Laboratory and Mobil Oil Company for the open data and also would kike to thank the valuable comments from the Associate Editor and three anonymous reviewers.

REFERENCES

[1] J. Yu and B. Wu, "Attention and hybrid loss guided deep learning for consecutively missing seismic data reconstruction," *IEEE Trans. Geosci. Remote Sens.*, vol. 60, pp. 1–8, 2021.

[2] N. Liu, L. Wu, J. Wang, H. Wu, J. Gao, and D. Wang, "Seismic data reconstruction via wavelet-based residual deep learning," *IEEE Trans. Geosci. Remote Sens.*, vol. 60, 2022, Art. no. 4508213.

[3] B. Wang, N. Zhang, W. Lu, and J. Wang, "Deep-learning-based seismic data interpolation: A preliminary result," *Geophysics*, vol. 84, no. 1, pp. V11–V20, Jan. 2019.

[4] X. Niu, L. Fu, W. Zhang, and Y. Li, "Seismic data interpolation based on simultaneously sparse and low-rank matrix recovery," *IEEE Trans. Geosci. Remote Sens.*, vol. 60, pp. 1–13, 2021.

[5] N. Liu, F. Li, D. Wang, J. Gao, and Z. Xu, "Ground-roll separation and attenuation using curvelet-based multichannel variational mode decomposition," *IEEE Trans. Geosci. Remote Sens.*, vol. 60, pp. 1–14, 2021.

[6] T. Zhong, Y. Li, N. Wu, P. Nie, and B. Yang, "Statistical analysis of background noise in seismic prospecting," *Geophys. Prospecting*, vol. 63, no. 5, pp. 1161–1174, 2015.

[7] M. Zhang, Y. Liu, and Y. Chen, "Unsupervised seismic random noise attenuation based on deep convolutional neural network," *IEEE Access*, vol. 7, pp. 179810–179822, 2019.

[8] L. Yang, W. Chen, W. Liu, B. Zha, and L. Zhu, "Random noise attenuation based on residual convolutional neural network in seismic datasets," *IEEE Access*, vol. 8, pp. 30271–30286, 2020.

[9] L. Guo, R. Luo, X. Li, Y. Zhou, T. Juanjuan, and C. Lei, "Seismic random noise removal based on a multiscale convolution and densely connected network for noise level evaluation," *IEEE Access*, vol. 10, pp. 13911–13925, 2022.

[10] N. Liu, J. Gao, B. Zhang, Q. Wang, and X. Jiang, "Self-adaptive generalized S-transform and its application in seismic time–frequency analysis," *IEEE Trans. Geosci. Remote Sens.*, vol. 57, no. 10, pp. 7849–7859, Oct. 2019.

[11] F. Li, H. Zhou, Z. Wang, and X. Wu, "ADDCNN: An attention-based deep dilated convolutional neural network for seismic facies analysis with interpretable spatial–spectral maps," *IEEE Trans. Geosci. Remote Sens.*, vol. 59, no. 2, pp. 1733–1744, Feb. 2021.

[12] F. Li, B. Lyu, J. Qi, S. Verma, and B. Zhang, "Seismic coherence for discontinuity interpretation," *Surveys Geophys.*, vol. 42, no. 6, pp. 1229–1280, Nov. 2021.

[13] Y. Lou, B. Zhang, R. Wang, T. Lin, and D. Cao, "Seismic fault attribute estimation using a local fault model," *Geophysics*, vol. 84, no. 4, pp. O73–O80, Jul. 2019.

[14] Y. Ao, W. Lu, B. Jiang, and P. Monkam, "Seismic structural curvature volume extraction with convolutional neural networks," *IEEE Trans. Geosci. Remote Sens.*, vol. 59, no. 9, pp. 7370–7384, Sep. 2021.

[15] J. Qi, B. Zhang, B. Lyu, and K. Marfurt, "Seismic attribute selection for machine-learning-based facies analysischoosing the best seismic attributes," *Geophysics*, vol. 85, no. 2, pp. O17–O35, 2020.

[16] Y. Lou, S. Li, S. Li, N. Liu, and B. Zhang, "Seismic volumetric dip estimation via multichannel deep learning model," *IEEE Trans. Geosci. Remote Sens.*, vol. 60, 2022, Art. no. 4511014.

[17] H. Wu, B. Zhang, T. Lin, D. Cao, and Y. Lou, "Semiautomated seismic horizon interpretation using the encoder–decoder convolutional neural network," *Geophysics*, vol. 84, no. 6, pp. B403–B417, Nov. 2019.

[18] Y. Lou, B. Zhang, T. Lin, and D. Cao, "Seismic horizon picking by integrating reflector dip and instantaneous phase attributes," *Geophysics*, vol. 85, no. 2, pp. O37–O45, Mar. 2020.

[19] S. Li, N. Liu, F. Li, J. Gao, and J. Ding, "Automatic fault delineation in 3-D seismic images with deep learning: Data augmentation or ensemble learning?" *IEEE Trans. Geosci. Remote Sens.*, vol. 60, 2022, Art. no. 5911214.

[20] G. Li, Y. Qiao, Y. Zheng, Y. Li, and W. Wu, "Semi-supervised learning based on generative adversarial network and its applied to lithology recognition," *IEEE Access*, vol. 7, pp. 67428–67437, 2019.

[21] J. Zhang, J. Li, X. Chen, and Y. Li, "Seismic lithology/fluid prediction via a hybrid ISD-CNN," *IEEE Geosci. Remote Sens. Lett.*, vol. 18, no. 1, pp. 13–17, Jan. 2021.

[22] N. Liu, T. Huang, J. Gao, Z. Xu, D. Wang, and F. Li, "Quantum-enhanced deep learning-based lithology interpretation from well logs," *IEEE Trans. Geosci. Remote Sens.*, vol. 60, pp. 1–13, 2021.

[23] G. Liu, C. Li, Z. Guo, and Y. Rao, "Irregularly sampled seismic data reconstruction using multiscale multidirectional adaptive prediction-error filter," *IEEE Trans. Geosci. Remote Sens.*, vol. 57, no. 5, pp. 2909–2919, May 2019.

[24] S. Fomel, "Seismic reflection data interpolation with differential offset and shot continuation," *Geophysics*, vol. 68, no. 2, pp. 733–744, 2003.

[25] B. Liu and M. D. Sacchi, "Minimum weighted norm interpolation of seismic records," *Geophysics*, vol. 69, no. 6, pp. 1560–1568, 2004.

[26] C. Li, G. Liu, Z. Hao, S. Zu, F. Mi, and X. Chen, "Multidimensional seismic data reconstruction using frequency-domain adaptive prediction-error filter," *IEEE Trans. Geosci. Remote Sens.*, vol. 56, no. 4, pp. 2328–2336, Apr. 2018.

[27] S. Spitz, "Seismic trace interpolation in the $F - X$ domain," *Geophysics*, vol. 56, no. 6, pp. 785–794, Jun. 1991.

[28] N. Gülünay, "Seismic trace interpolation in the Fourier transform domain," *Geophysics*, vol. 68, no. 1, pp. 355–369, 2003.

[29] K. Chen and M. D. Sacchi, "Robust reduced-rank filtering for erratic seismic noise attenuation," *Geophysics*, vol. 80, no. 1, pp. V1–V11, Jan. 2015.

[30] H. H. Lari, M. Naghizadeh, M. D. Sacchi, and A. Gholami, "Adaptive singular spectrum analysis for seismic denoising and interpolation," *Geophysics*, vol. 84, no. 2, pp. V133–V142, Mar. 2019.

[31] N. Liu, J. Wang, J. Gao, K. Yu, Y. Lou, Y. Pu, and S. Chang, "NS2NS: Self-learning for seismic image denoising," *IEEE Trans. Geosci. Remote Sens.*, vol. 60, 2022, Art. no. 5922311.

[32] X. Dong and Y. Li, "Denoising the optical fiber seismic data by using convolutional adversarial network based on loss balance," *IEEE Trans. Geosci. Remote Sens.*, vol. 59, no. 12, pp. 10544–10554, Dec. 2020.

[33] X. Wu, S. Yan, J. Qi, and H. Zeng, "Deep learning for characterizing paleokarst collapse features in 3-D seismic images," *J. Geophys. Res., Solid Earth*, vol. 125, no. 9, 2020, Art. no. e2020JB019685.

[34] B. Zhang, Y. Pu, Z. Xu, N. Liu, S. Li, and F. Li, "Exploring factors affecting the performance of deep learning in seismic fault attribute computation," *Interpretation*, vol. 10, no. 4, pp. 1–75, 2022.

[35] X. Dong, J. Lin, S. Lu, X. Huang, H. Wang, and Y. Li, "Seismic shot gather denoising by using a supervised-deep-learning method with weak dependence on real noise data: A solution to the lack of real noise data," *Surveys Geophys.*, vol. 43, pp. 1–32, Oct. 2022.

[36] N. Liu, J. Wang, J. Gao, S. Chang, and Y. Lou, "Similarity-informed self-learning and its application on seismic image denoising," *IEEE Trans. Geosci. Remote Sens.*, vol. 60, pp. 1–13, 2022.

[37] Y. Jia and J. Ma, "What can machine learning do for seismic data processing? An interpolation application," *Geophysics*, vol. 82, no. 3, pp. V163–V177, May 2017.

[38] X. Chai, G. Tang, S. Wang, R. Peng, W. Chen, and J. Li, "Deep learning for regularly missing data reconstruction," *IEEE Trans. Geosci. Remote Sens.*, vol. 58, no. 6, pp. 4406–4423, Jun. 2020.

[39] H. Kaur, N. Pham, and S. Fomel, "Seismic data interpolation using deep learning with generative adversarial networks," *Geophys. Prospecting*, vol. 69, no. 2, pp. 307–326, Feb. 2021.

[40] X. Li, B. Wu, X. Zhu, and H. Yang, "Consecutively missing seismic data interpolation based on coordinate attention unet," *IEEE Geosci. Remote Sens. Lett.*, vol. 19, pp. 1–5, 2021.

[41] Q. Liu, L. Fu, and M. Zhang, "Deep-seismic-prior-based reconstruction of seismic data using convolutional neural networks," *Geophysics*, vol. 86, no. 2, pp. V131–V142, Mar. 2021.

[42] Y. Wang, B. Wang, N. Tu, and J. Geng, "Seismic trace interpolation for irregularly spatial sampled data using convolutional autoencoder," *Geophysics*, vol. 85, no. 2, pp. V119–V130, Mar. 2020.

[43] O. Ronneberger, P. Fischer, and T. Brox, "U-Net: Convolutional networks for biomedical image segmentation," in *Proc. Int. Conf. Med. Image Comput. Comput.-Assist. Intervent.* Cham, Switzerland: Springer, 2015, pp. 234–241.

[44] H. Wu, B. Zhang, and N. Liu, "Self-adaptive denoising net: Self-supervised learning for seismic migration artifacts and random noise attenuation," *J. Petroleum Sci. Eng.*, vol. 214, Jul. 2022, Art. no. 110431.

[45] X. Wu, L. Liang, Y. Shi, and S. Fomel, "FaultSeg3D: Using synthetic data sets to train an end-to-end convolutional neural network for 3D seismic fault segmentation," *Geophysics*, vol. 84, no. 3, pp. IM35–IM45, May 2019.

[46] N. Liu, T. He, Y. Tian, B. Wu, J. Gao, and Z. Xu, "Common-azimuth seismic data fault analysis using residual UNet," *Interpretation*, vol. 8, no. 3, pp. SM25–SM37, Aug. 2020.

[47] Y. Yang, Y. Lei, N. Liu, Z. Wang, J. Gao, and J. Ding, "SparseTFNet: A physically informed autoencoder for sparse time–frequency analysis of seismic data," *IEEE Trans. Geosci. Remote Sens.*, vol. 60, 2022, Art. no. 4512812.

[48] X. Chai, H. Gu, F. Li, H. Duan, X. Hu, and K. Lin, "Deep learning for irregularly and regularly missing data reconstruction," *Sci. Rep.*, vol. 10, no. 1, pp. 1–18, 2020.

[49] T. He, B. Wu, and X. Zhu, "Seismic data consecutively missing trace interpolation based on multistage neural network training process," *IEEE Geosci. Remote Sens. Lett.*, vol. 19, pp. 1–5, 2021.

[50] W. Fang, L. Fu, M. Zhang, and Z. Li, "Seismic data interpolation based on U-Net with texture lossu-net with texture loss for interpolation," *Geophysics*, vol. 86, no. 1, pp. V41–V54, 2021.

[51] Y. Xiao, X. Su, Q. Yuan, D. Liu, H. Shen, and L. Zhang, "Satellite video super-resolution via multiscale deformable convolution alignment and temporal grouping projection," *IEEE Trans. Geosci. Remote Sens.*, vol. 60, pp. 1–19, 2021.

[52] Y. Xiao, Q. Yuan, J. He, Q. Zhang, J. Sun, X. Su, J. Wu, and L. Zhang, "Space-time super-resolution for satellite video: A joint framework based on multi-scale spatial–temporal transformer," *Int. J. Appl. Earth Observ. Geoinf.*, vol. 108, Apr. 2022, Art. no. 102731.

[53] J. Wang, K. Sun, T. Cheng, B. Jiang, C. Deng, Y. Zhao, D. Liu, Y. Mu, M. Tan, X. Wang, and W. Liu, "Deep high-resolution representation learning for visual recognition," *IEEE Trans. Pattern Anal. Mach. Intell.*, vol. 43, no. 10, pp. 3349–3364, Oct. 2020.

[54] T. Chai and R. R. Draxler, "Root mean square error (RMSE) or mean absolute error (MAE)?—Arguments against avoiding RMSE in the literature," *Geosci. Model Develop.*, vol. 7, no. 3, pp. 1247–1250, Jun. 2014.

[55] Z. Wang, A. C. Bovik, H. R. Sheikh, and E. P. Simoncelli, "Image quality assessment: From error visibility to structural similarity," *IEEE Trans. Image Process.*, vol. 13, no. 4, pp. 600–612, Apr. 2004.

[56] Q. Wei, X. Li, and M. Song, "Reconstruction of irregular missing seismic data using conditional generative adversarial networks," *Geophysics*, vol. 86, no. 6, pp. V471–V488, Nov. 2021.

[57] V. Nair and G. E. Hinton, "Rectified linear units improve restricted Boltzmann machines," in *Proc. ICML*, 2010, pp. 807–814.

[58] D. M. Allen, "Mean square error of prediction as a criterion for selecting variables," *Technometrics*, vol. 13, no. 3, pp. 469–475, 1971.

SHENGJUN LI received the B.S. degree in geophysical prospecting and information technology from the China University of Petroleum, Dongying, Shandong, China, in 2007, and the Ph.D. degree in geologic resource exploitation projects form the China University of Petroleum, Beijing, China, in 2021. He is currently a Senior Engineer with the Research Institute of Petroleum Exploration and Development-Northwest, PetroChina, Lanzhou, Gansu, China. His research interests include attribute analysis and parameter inversion, seismic wave propagation, and reservoir prediction.

JIANHU GAO received the B.S. degree in geophysical prospecting and information technology from the China University of Petroleum, Beijing, China, in 2000, and the Ph.D. degree in solid earth geophysics from the Institute of Geology and Geophysics, Chinese Academy of Sciences, Beijing, in 2008. He is currently with the Petroleum Exploration and Development Research Institute-Northwest Branch, PetroChina, Lanzhou, Gansu, China. His research interests include seismic reservoir prediction, rock physics, and deep learning.

JINYONG GUI received the B.S. degree in geophysical prospecting and information technology from the China University of Petroleum (East China), Qingdao, Shandong, China, in 2012, where he is currently pursuing the Ph.D. degree in energy source and environment protection. He is also with the Petroleum Exploration and Development Research Institute, Northwest Branch, PetroChina, Lanzhou, Gansu, China. His research interests include seismic inversion, reservoir prediction and fluid identification, and deep learning.

LUKUN WU received the B.Eng. degree in land engineering from Changn University, Xi'an, Shaanxi, China, in 2021. He is currently pursuing the master's degree with the School of Software Engineering, Xi'an Jiaotong University, Xi'an. His research interests include machine learning and deep learning, seismic data reconstruction, self-supervised and unsupervised algorithms, and seismic random noise attenuation.

NAIHAO LIU (Member, IEEE) received the B.S. degree in communication engineering from Jilin University, Changchun, Jilin, China, in 2012, and the Ph.D. degree in information and communication engineering form Xi'an Jiaotong University, Xi'an, Shaanxi, China, in 2018. From 2017 to 2018, he was visited the Department of Geological Sciences, The University of Alabama, Tuscaloosa, AL, USA. He is currently with the School of Information and Communications Engineering, Xi'an Jiaotong University. His research interests include seismic time-frequency analysis, multi-attribute analysis and parameter inversion, deep learning, and reservoir characterization.

DONGYANG HE received the master's degree in geological resources and geological engineering from the China University of Petroleum (East China), in 2019. He is currently with the Institute of Geophysics, Northwest Branch of China Petroleum Exploration and Development Research Institute. His research interests include signal processing, seismic inversion, and software development.

XIN GUO received the B.S. degree in exploration technology and engineering from the China University of Petroleum (East China), in 2013, and the master's degree majoring in earth exploration and information engineering from the Petroleum Exploration and Development Research Institute, in 2016. He is currently with the China Petroleum Exploration and Development Research Institute, Northwest, (NWGI), and engage in researches on seismic high-resolution processing and reservoir prediction.